THE JOURNAL OF PHYSICAL CHEMISTRY C
A JOURNAL OF THE AMERICAN CHEMICAL SOCIETY

pubs.acs.org/JPCC

Article

Stabilization of Plasmonic Silver Nanostructures with Ultrathin Oxide Coatings Formed Using Atomic Layer Deposition

Arin S. Preston, Robert A. Hughes, Nathaniel L. Dominique, Jon P. Camden, and Svetlana Neretina*

Cite This: *J. Phys. Chem. C* 2021, 125, 17212–17220

Read Online

ACCESS | Metrics & More | Article Recommendations | Supporting Information

ABSTRACT: Even though performance metrics position silver as the preeminent plasmonic material in the visible and near-infrared regions of the electromagnetic spectrum, it remains underutilized in applications because its properties irreversibly degrade in the environments it must operate. The emergence of shell-isolated plasmonic nanostructures as a distinct class of nanomaterials has, however, created new opportunities for the utilization of silver because its vulnerable surfaces can be encapsulated in a chemically robust transparent shell while maintaining important plasmonic properties. To fully capitalize on this opportunity requires that shell−nanostructure combinations be rationally designed where consideration is given to a parameter space encompassing nanostructure stability−property relationships. Herein, we demonstrate the layer-by-layer deposition capabilities of the atomic layer deposition (ALD) technique as a means to design shell-isolated silver nanostructures where the confined structure acts as a built-in plasmonic sensor for spectroscopically evaluating durability in air, water, and chemically aggressive environments. For all cases, appropriately designed oxide shells are shown to provide long-term stability, but where their own surface chemistry and structural integrity become limiting factors in bolstering and preserving plasmonic properties. The work, therefore, forwards the use of ALD-deposited layers for the realization of shell-isolated plasmonic nanostructures that exploit the remarkable properties of silver.

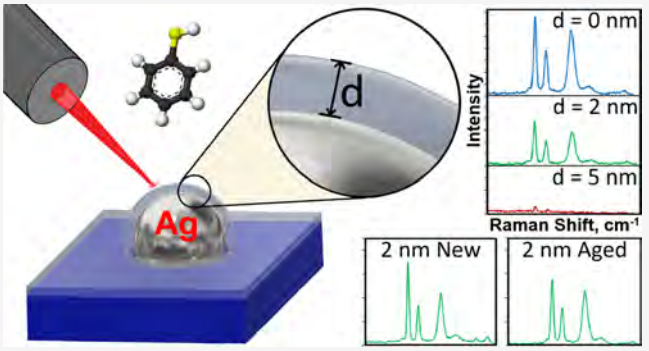

INTRODUCTION

The encapsulation of a plasmonic nanostructure within an ultrathin pinhole-free dielectric shell leads to large-scale disruptions in its optical response. Even though such influences are often considered detrimental to nanostructure functionality, the newfound properties associated with these so-called shell-isolated plasmonic nanostructures can prove highly advantageous. When confined within a shell, a plasmonic nanostructure can (i) avoid oxidation, (ii) endure chemically aggressive environments, (iii) attain biocompatibility, (iv) maintain its shape at elevated temperatures, (v) have an extended shelf life, (vi) become highly recyclable, (vii) eliminate aggregation in liquid media, (viii) be tuned to a precise resonance through fine adjustments to the local dielectric environment, (ix) display altered photochemistry brought on by synergistic interactions with the shell material, (x) prevent unwanted electron transfer processes to adjacent materials, (xi) extend the lifetime of hot electrons through their injection into the conduction band of a semiconducting shell, and (xii) form nanogaps with other plasmonic structures with a width that is precisely set by the shell dimensions. As a result, shell-isolated plasmonic nanostructures have emerged as a distinct class of nanomaterials with functionalities that are of high relevance to applications in shell-isolated nanoparticle-enhanced Raman spectroscopy,[1−4] plasmon-enhanced fluorescence,[5,6] refractory plasmonics,[7−9] photoelectrocatalysis,[3] nanoelectronics,[3] and photovoltaics.[3]

As a plasmonic material, Ag has unrivaled properties across the visible and near-infrared regions of the electromagnetic spectrum. Its performance is attributable to low levels of plasmonic damping when compared to more lossy metals such as Au and Cu. As such, Ag nanostructures exhibit sharper and more intense localized surface plasmon resonances (LSPRs), stronger near-field intensities, and the largest quality factors.[10,11] Given that nanostructure shape and size control is a prerequisite for achieving tunable plasmonic resonances, it is not surprising that there is now extensive literature dedicated to the formation of colloidal and substrate-supported Ag nanostructures using liquid-state syntheses,[12−14] vapor phase self- and directed-assembly processes,[15−17] and lithographic techniques.[18,19] Despite these extraordinary properties and capabilities, the prominence of Ag as a plasmonic material is

Received: May 25, 2021
Revised: June 30, 2021
Published: July 28, 2021

https://doi.org/10.1021/acs.jpcc.1c04599
J. Phys. Chem. C 2021, 125, 17212−17220

one that is greatly diminished by its deficiencies that include poor chemical stability, irreversible morphological transformations, and a lack of biocompatibility. In air, Ag readily tarnishes where sensitivities to oxygen,[20−22] sulfur,[18,23,24] humidity,[25,26] and carbon[20,27] have all been documented. In aqueous environments, Ag can undergo chemical and morphological disruptions due to dissolved oxygen,[28,29] pH,[30] and halide ions.[28,31,32] Nanostructure degradation also occurs under illumination[21,32] and heat.[8,25,33] All of these factors lead to irreversible damage to Ag nanostructures that can manifest themselves as (i) LSPR dampening, broadening, and red shifting, (ii) severely compromised plasmonic near-field intensities, and (iii) morphological transformations. As a consequence, Ag is widely regarded as being inferior to Au for plasmonic applications. This, however, does not have to be the case for applications related to shell-isolated plasmonic nanostructures, provided that the Ag nanostructures are encased in a suitably designed shell that is able to mitigate weaknesses while maintaining functionality in the operating environment in which it is expected to perform.

Numerous strategies have been forwarded for protecting Ag nanostructures against application-specific working environments.[34] Methods for preserving colloids rely on the formation of protective layers that passivate an otherwise reactive surface. Oxides,[35,36] metals,[32,37] polymers,[38,39] short-chain alkanethiols,[40,41] and aliphatic amines[42] have all been used for this purpose and provide varying degrees of protection. Methods for protecting substrate-supported structures can encapsulate structures individually or form a continuous layer over both the nanostructures and the exposed substrate. Oxides,[8,43−46] nitrides,[47] graphene,[48,49] hydrogen silsesquioxane,[50] hexathiols,[18] and hydrogen terminating layers[19] have all demonstrated their effectiveness in preserving Ag under particular conditions. Building upon these achievements will, however, require that the various protective layers be better understood in terms of their limitations in a wide variety of application-based working environments, their influence upon plasmonic properties, and whether they are subjected to their own adverse aging characteristics.

Atomic layer deposition (ALD)[51] is a technique that has been widely used to apply protective claddings to vulnerable surfaces. It offers a significant advantage in that it allows for the application of uniform conformal coatings to intricately shaped objects in a layer-by-layer manner. Low-temperature ALD-deposited oxides represent a particularly intriguing class of cladding materials for plasmonic nanostructures since they are optically transparent, chemically stable, highly impermeable, and able to withstand high temperatures. Numerous demonstrations exist where clad metals in the form of substrate-supported nanostructures, films, and bulk surfaces have withstood chemical and thermal environments that would otherwise prove impossible.[7−9,43−46,52−54] Given that many oxides are amenable to ALD depositions where there exist exacting controls over layer thicknesses, there is the potential to design claddings that provide protection to vulnerable metal surfaces while simultaneously allowing them to perform optimally as plasmonic materials. Herein, a systematic study is presented in which three different ALD-deposited oxide claddings (i.e., HfO_2, Al_2O_3, and TiO_2) are examined for their ability to sustain the plasmonic properties of substrate-based Ag nanostructures in air, H_2O, and chemically aggressive environments for time intervals lasting up to 200 days. Our findings reveal that ALD cladding technologies provide a viable route for forming shell-isolated nanostructures that chemically passivate Ag surfaces while still being able to support important plasmonic properties.

EXPERIMENTAL METHODS

Materials. Ag sputter targets were cut from 0.5 mm thick foils with 99.9985% purity (Alfa Aesar). Two-side polished [0001]-oriented sapphire substrates with a 100 mm diameter and 0.65 mm thickness were obtained from MTI Corp. and diced into 5 mm × 10.5 mm pieces. Ultrahigh purity Ar gas (Airgas) was used for all dewetting procedures. The ALD precursors tetrakis(ethylmethylamido)hafnium (TEMAH) and trimethylaluminum (TMA) were sourced from MilliporeSigma while tetrakis(dimethylamido)titanium (TDMAT) was obtained from SAFC Hitech. Durability tests were carried out using nitric acid (HNO_3, Alfa Aesar) and sodium hydroxide (NaOH, MilliporeSigma). Surface-enhanced Raman spectroscopy (SERS) measurements used benzenethiol (i.e., thiophenol) (≥99%, Sigma-Aldrich). Deionized (DI) H_2O with a resistivity of 18.2 MΩ·cm was used for the preparation of all aqueous solutions. All chemicals were used as received.

Synthesis of Ag Nanoparticles. Thin films of Ag, with a thickness of 3 nm, are sputter deposited onto sapphire substrates at room temperature, after which they are transferred to a quartz tube furnace equipped with air-tight fittings. The air within the tube is then purged for 30 min with Ar at a flow rate of 120 $cm^3 \cdot min^{-1}$. The flow rate is then reduced to 60 $cm^3 \cdot min^{-1}$, followed by a dewetting procedure in which the sample is heated to 700 °C in 20 min and cooled to room temperature in 30 min. Once removed from the tube furnace, the samples were transferred either to an ALD deposition system or for studies involving bare samples, immediately subjected to durability testing.

Atomic Layer Deposition. Oxide claddings were deposited using growth parameters that are described in detail elsewhere.[7] Briefly, TEMAH, TMA, and TDMAT gases act as Hf, Al, and Ti precursors for self-limiting half-reactions that are completed upon exposure to H_2O vapor. Such growth cycles are carried out in a pulsed, alternating, and nonoverlapping manner, where each is separated by an N_2 gas purge. The metal precursor, H_2O, and N_2 purge exposure times were optimized for HfO_2 (150 ms, 20 ms, 10 s), Al_2O_3 (20 ms, 20 ms, 7 s), and TiO_2 (800 ms, 1 s, 7 s) depositions. The TiO_2 deposition also differed in that a 3 s pumping interval occurred after each N_2 purge. All ALD depositions were carried out at 200 °C. These growth conditions resulted in deposition rates of 0.9, 1.0, and 0.25 Å/cycle for HfO_2, Al_2O_3, and TiO_2, respectively.

SERS Measurements. Samples for SERS characterization were prepared by drop-casting 5 μL of 10 mM thiophenol in methanol, air-dried, and inverted between two microscope slides. Even though thiols have no affinity for the Al_2O_3 surface,[55] this procedure does lead to their physisorption.[56] The 2 nm thick pinhole-free ALD coatings used for SERS characterization were prepared using methods described previously[7] in which a 5 nm thick Al_2O_3 layer was deposited followed by the removal of 3 nm using a 1 mM NaOH etch. SERS characterization was carried out using a home-built setup in which a 633 nm HeNe laser (Thorlabs) is first directed into an inverted microscope (Nikon Ti-U) and then focused onto a substrate with an objective lens (20×, NA = 0.5). The scattered light is then collected through the same objective lens, filtered through a Rayleigh rejection filter (Semrock), and fed into a spectrometer (Princeton Instruments Acton SP2300,

https://doi.org/10.1021/acs.jpcc.1c04599
J. Phys. Chem. C 2021, 125, 17212−17220

f = 0.3 mm, 1200 g·mm^{-1}). Spectra, taken with a 60 s exposure time, were analyzed using Winspec/32 software (Princeton Instruments). In general, five SERS spectra were acquired and averaged. Baseline subtraction was performed using an Igor Multipeak fit 2.0 peak fitting algorithm using Gaussian peaks and a log poly 5 curve to model the Raman and background signals, respectively. The background spectra showed four strong peaks at 420, 750, 1370, and 1400 cm^{-1}.[57]

Instrumentation. Sputter depositions were carried out in a model 681 Gatan high resolution ion beam coater. Dewetting procedures utilized a Lindberg Blue M quartz tube furnace. ALD depositions of Al_2O_3 and HfO_2 were performed using a Cambridge Savannah S100 system, while TiO_2 depositions utilized an Oxford FlexAl system. Coating thicknesses were measured with Gaertner L116S ellipsometer. LSPR extinction spectra were recorded using a JASCO V-730 UV−Visible spectrophotometer. Scanning electron microscopy (SEM) images were obtained using a Helios G4 Ux SEM/FIB workstation (FEI). An 18 W VWR UV hand lamp operating at 254 nm was used to obtain the data in Figures 2e and S2.

RESULTS

Preparation of Oxide-Clad Ag Nanostructures. Oxide-clad Ag nanostructures were prepared using a three-step process in which (i) a 3 nm thick Ag film is sputter deposited onto a sapphire substrate, (ii) heated in Ar to temperatures sufficient to promote solid-state dewetting,[17,58] and (iii) coated with a conformal oxide layer using ALD (Figure 1a). The dewetting process results in nanostructures shaped as truncated spheres that express a single-crystal character.[58,59] The structures, which are formed at a density of approximately 3 × 10^{10} cm^{-2}, have randomized placement on the substrate and a broad size distribution where the average diameter is 25 nm (Figures 1b and S1). The structures exhibit an intense LSPR resonance dipole peak centered near 450 nm and a smaller quadrupole peak near 350 nm (Figure 1c, black curve), a response that is determined by nanostructure size, shape, and the asymmetric dielectric environment imposed by the substrate.[16,60,61] ALD-deposited oxide claddings of HfO_2, Al_2O_3, and TiO_2 were applied to the dewetted nanostructures as well as to the intervening spaces between the structures using TEMAH, TMA, and TDMAT precursors, respectively. For each case, H_2O was used as the oxidant. HfO_2 and Al_2O_3 were deposited to a thickness of 5 nm, while the TiO_2 deposition was halted at 3 nm. The thicknesses were chosen on the basis of prior work showing that they are the thinnest pinhole-free claddings achievable under the growth conditions used.[7] As is typical for ALD-deposited refractory oxides, the coatings are amorphous where their exact composition can deviate from the stoichiometric ratio. As the oxide is applied to the Ag nanostructures, the plasmon resonance peak undergoes a red shift (Figure 1c, blue, purple, and red curves), the degree to which is dependent on the cladding thickness and its index of refraction.[62,63] Oxide-clad Ag nanostructures produced in this manner were immediately subjected to durability testing under various environmental conditions where oxide-free structures were similarly assessed so as to provide a baseline metric against which their performance was measured.

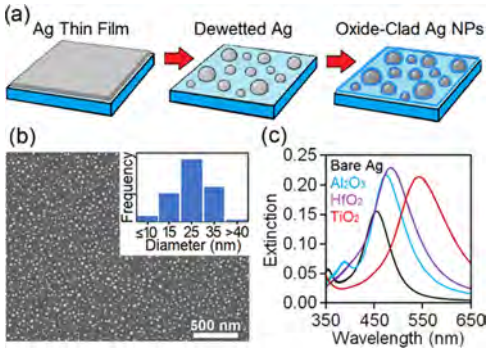

Figure 1. (a) Schematic of the three-stage process used to prepare oxide-clad Ag nanostructures. (b) SEM image of substrate-bound Ag nanostructures prepared using solid-state dewetting and a histogram of their size distribution. (c) Extinction spectra showing the LSPR of bare Ag nanostructures and identical structures after the application of HfO_2 (5 nm), Al_2O_3 (5 nm), and TiO_2 (3 nm) claddings.

Oxide-Clad Ag Exposed to Air. With the recognition that ambient conditions are the most likely environment under which on-chip plasmonic materials must operate, the long-term stability of clad Ag nanostructures was assessed over a 200-day period. For these studies, four nominally identical samples were prepared by dewetting Ag films, after which oxide coatings of HfO_2, Al_2O_3, and TiO_2 were immediately applied to three of the samples while the fourth was left bare. The air-stability of the structures was then evaluated by monitoring spectroscopic shifts in the plasmon resonance, where the duration between measurements was continually adjusted depending on the degree of change observed since the prior experiment. Between the measurements, samples were stored in an open-air environment and were, hence, susceptible to naturally occurring fluctuations in humidity, temperature, and lighting conditions as well as airborne contaminants.

Figure 2a shows the time dependence of the extinction spectrum for bare Ag nanostructures over an 86-day duration. The data reveals that the prolonged exposure to air causes an

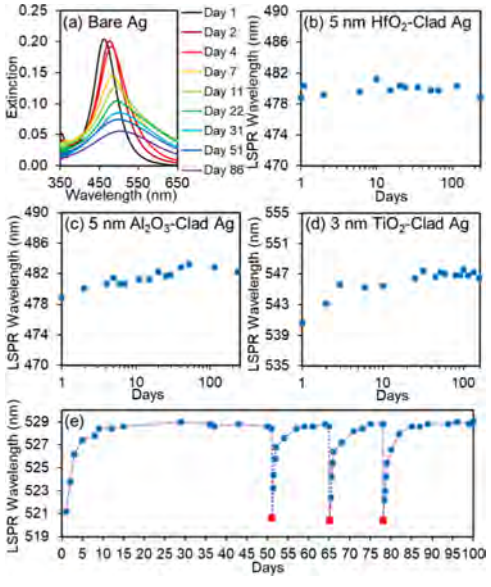

Figure 2. (a) Time-dependent extinction spectra for bare Ag nanostructures stored under ambient conditions. Time dependence of the LSPR wavelength for Ag nanostructures clad with (b) 5 nm HfO_2, (c) 5 nm Al_2O_3, and (d) 3 nm TiO_2. (e) Time dependence of the LSPR wavelength for TiO_2-clad Ag nanostructures that were allowed to age in air except for their intermittent exposure to UV light on days denoted by the red symbols.

https://doi.org/10.1021/acs.jpcc.1c04599
J. Phys. Chem. C 2021, 125, 17212−17220

initially intense plasmon resonance to weaken as it broadens and red-shifts. The rate of degradation is most acute for the first seven days, after which it lessens considerably. Such behavior is consistent with a shell of tarnished material offering some degree of protection to the innermost Ag. The red shift is caused by the altered dielectric environment in which the encapsulated Ag is enveloped. Although these single-crystal nanostructures show significant degradation, they are notably more stable than patterned polycrystalline structures derived from room temperature Ag depositions[25] as well as similarly formed patterned structures that were subsequently annealed at 180 °C.[24]

In stark contrast to the bare nanostructures, the oxide-clad Ag structures show a high degree of stability in the LSPR peak position over the 200-day duration studied (Figure 2b–d). This is as anticipated since refractory oxides exhibit low oxygen self-diffusion coefficients. A closer inspection, however, reveals that while the HfO_2-passivated Ag nanostructures show no appreciable shifts in the LSPR, the Al_2O_3-clad Ag structures exhibit a red shift of nearly 3 nm over the first 50-day interval before settling, while the TiO_2-clad structures show a relatively rapid 5 nm shift followed by a slower 2 nm shift before stabilizing after 20 days. With the understanding that shifts in the LSPR are induced by changes to the dielectric environment in the vicinity of the Ag nanoparticle, possible origins for these slight shifts include light-induced reactions leading to a modified oxide-metal interface, densification of the amorphous oxide, sensitivity to humidity, or the accumulation of adsorbates on the oxide surface. To further investigate this aspect, the LSPR of TiO_2-clad Ag nanostructures was monitored over a 100-day period (Figure 2e), where on three separate occasions, denoted by the red symbols, the sample was illuminated with UV light for 10 min after which its LSPR response was immediately measured. The data reveals that the red shift associated with aging is reversible upon UV light exposure. The reversible nature provides compelling indirect evidence for the red shift being caused by the adsorption of airborne contaminants, an assignment that is supported by the fact that TiO_2-clad Au nanostructures show similar behavior (Figure S2). The removal of adsorbed contaminants with UV light is consistent with the use of TiO_2 as a self-cleaning photocatalyst.[44] Together, these results show that all three oxides effectively passivate an otherwise reactive Ag surface but where the oxide itself can undergo subtle changes.

For the studies presented in Figure 2, the cladding thicknesses were chosen to ensure the pinhole-free encapsulation of the Ag nanostructures. Such configurations offer protection to Ag when placed in etchants (vide infra). This degree of protection, however, has a downside in that the plasmonic near fields emanating from resonantly excited structures are severely diminished over the spatial extent of the coating.[7] It therefore becomes a point of interest as to whether a much thinner coating, which has a small number of pinholes, still offers sufficient protection to significantly enhance the durability of the Ag nanostructures while allowing for significantly larger near fields. As such, an investigation was carried out in which the LSPR was monitored over a 35-day duration for ultrathin Al_2O_3 claddings. Figure 3 presents a progression of the time-dependent shifts in the LSPR as the cladding thickness is varied from 0 to 1 nm. It reveals a trend in which all structures undergo a rapid LSPR red shift in the first few days but where the degree of shift becomes almost

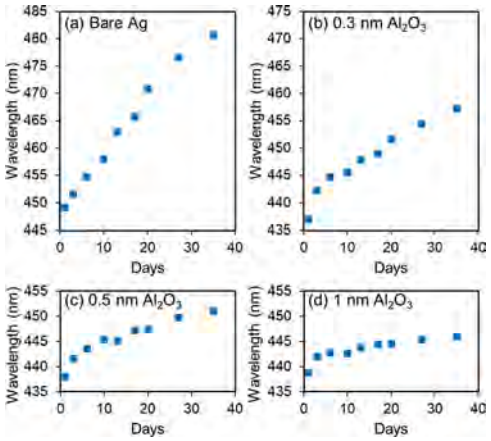

Figure 3. Time dependence of the LSPR wavelength for (a) bare Ag nanostructures under ambient conditions and for identical structures with (b) 0.3, (c) 0.5, and (d) 1 nm thick Al_2O_3 claddings.

negligible as the coating thickness is increased to 1 nm. Likewise, the long-term trend reveals that the Ag nanoparticle degradation is inhibited by the ultrathin oxide coating but where only the 1 nm thick sample shows a high degree of stabilization. The data, hence, indicates the potential for favorable trade-offs in terms of sacrificing some degree of Ag stability so as to gain an 80% reduction in cladding thickness.

Oxide-Clad Ag Exposed to Aqueous Environments. Given that numerous applications require that plasmonic materials operate within aqueous environments, studies were carried out to assess the durability of both bare and oxide-clad Ag nanostructures. With an entire literature dedicated to the synthesis of colloidal Ag nanostructures under aqueous conditions, it may seem counterintuitive that Ag nanostructures need protection from H_2O. When, however, truly bare Ag nanostructures, such as those formed through solid-state dewetting, are exposed to H_2O, they are highly susceptible to oxidative etching processes[64,65] that leach Ag,[28] an effect that is exasperated by the presence of halide ions.[28,31,32] Bare Ag nanostructures, hence, only show significant stability in aqueous media if the dissolved oxygen is removed from the H_2O using an inert gas purge.[28] Ag colloids are less prone to such effects because their synthesis necessitates the use of stabilizing agents that not only retard nanostructure agglomeration but also provide a degree of protection against oxidation within aqueous environments.[21,66] Moreover, a colloid of Ag nanostructures, when compared to their substrate-based counterparts, typically present orders of magnitude more structures to the aqueous media, and as a result, they are more slowly impacted by any oxidative etching processes because the number of dissolved oxygen molecules within the liquid, at any point in time, is typically outnumbered by Ag atoms. An understanding of these leaching processes and the extent to which oxide claddings can protect a small yet vulnerable, population of bare Ag nanostructures is therefore warranted.

Bare Ag nanostructures, as well as those clad with HfO_2, Al_2O_3, and TiO_2, were prepared, spectroscopically characterized in air, and then submerged in 10 mL of H_2O, where each of the four samples was placed in separate beakers. Under these conditions, the number of Ag atoms on the substrate surface (i.e., 9.2×10^{15}) is outnumbered by the dissolved oxygen within the H_2O (1.6×10^{18} O_2 molecules at 8.56 mg·

https://doi.org/10.1021/acs.jpcc.1c04599
J. Phys. Chem. C 2021, 125, 17212−17220

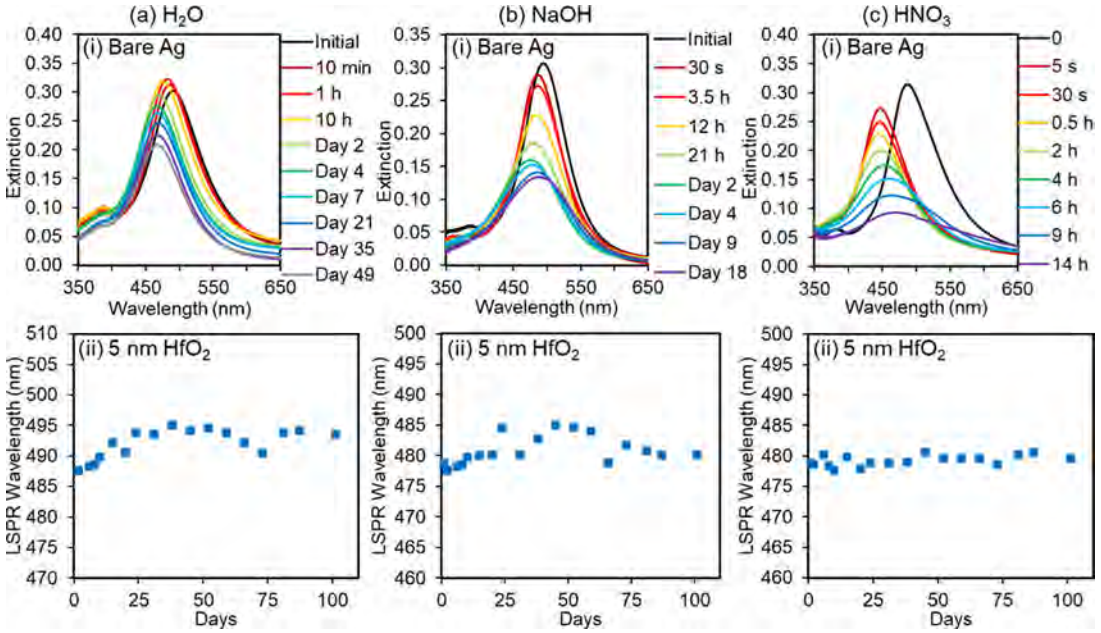

Figure 4. Time-dependent data showing (i) the degradation in the extinction characteristics of bare Ag nanostructures and (ii) a comparatively stable LSPR wavelength for identical Ag structures clad with 5 nm of HfO_2 when exposed to (a) H_2O, (b) 1 M NaOH, and (c) 1 M HNO_3.

L^{-1} for room temperature H_2O) by a factor of 175. All samples were periodically removed from their respective beakers, dried under an N_2 gas flow, spectroscopically characterized, and then reinserted back into the H_2O. During storage, all of the beakers were covered with glass slides to reduce dust exposure. H_2O evaporation was compensated for by topping off the liquid level where, at no point, was the level allowed to drop below 6 mL.

Figure 4a shows the time dependence of the extinction spectrum for bare Ag nanostructures upon exposure to H_2O for a 49-day duration. The Ag LSPR rapidly changes upon initial exposure to H_2O, after which change still occurs but at a much slower rate where the overall trend is for the spectra to blue-shift as the LSPR extinction maximum first rises and then falls. The rapid changes occurring immediately after H_2O exposure are caused by the loss of Ag from the nanostructure due to oxidative etching, a result consistent with prior studies that characterized the leaching of Ag from similarly formed structures using inductively coupled plasma optical emission spectrometry (ICP-OES).[28] As Ag is lost, the nanostructure is reduced in size, and, as expected, this gives rise to a blue shift in the LSPR. The initial rise and then fall in the LSPR extinction, which is accompanied by improvements in the H_2O stability of the nanostructures, is consistent with the formation of a protective Ag_2O layer around the remaining structure that is both insoluble in H_2O[67] and presents an altered dielectric environment.[68] Overall, these results demonstrate the vulnerability of bare Ag nanostructures in H_2O.

In sharp contrast to the air-durability results, the H_2O-durability of Ag nanostructures is not ensured by the application of all three cladding materials. The HfO_2 cladding performs well, showing a time-dependent LSPR that remains near-constant over most of the 100-day period investigated (Figure 4a, lower panel). The red shift in the LSPR observed in the first few weeks is likely attributable to changes in the dielectric environment around the clad structure, either through H_2O-induced changes to the cladding or the adsorption of contaminants to its surface. Al_2O_3- and TiO_2-clad Ag nanostructures showed significant deterioration in the LSPR properties (Figure S3a). The Al_2O_3-cladding performed the poorest, providing Ag with protection that abates after only a few days (Figure S3a). This is as anticipated since ALD-deposited Al_2O_3 layers are known to undergo a morphological disruption in H_2O[69] to the extent that a 5 nm cladding will eventually breach, exposing the underlying Ag to the deleterious influences of the aqueous environment. TiO_2-coated structures show a time-dependent LSPR that indicates that a breach in the cladding occurs on the time scale of several weeks, suggesting that it too undergoes a morphological reconfiguration in aqueous environments. Collectively, these results show that HfO_2 claddings provide optimal protection to Ag against aqueous environments.

With HfO_2-clad structures showing the capability to operate in H_2O for long durations, further durability testing was carried out in extreme pH environments. Bare Ag, when placed in a basic solution of 1 M NaOH, sees a rapid deterioration in its LSPR over the first few days, followed by a much slower rate of decay (Figure 4b). The LSPR wavelength initially blue-shifts but later reverses direction and red-shifts back to a value near its initial position. When bare structures are placed in an acidic solution of 1 M HNO_3, there is an almost immediate blue shift in the LSPR of 50 nm followed by a rapid deterioration where, once again, there exists a red shift at later times. The most likely explanation for this unexpected red shift is a nanostructure shape change that sees its roundish morphology become somewhat flattened. In such a scenario, the red-shifting influence caused by this flattening[16] more than compensates for the blue-shifting influence arising from a reduction in nanoparticle size. Identical Ag structures, when clad with 5 nm of HfO_2, are highly robust to these extreme pH environments, showing a near-constant LSPR wavelength over the 100-day duration studied (Figure 4b,c, lower panels). The result is consistent with prior work that has demonstrated HfO_2 as being robust in a variety of chemically aggressive environments.[53,70,71] Noteworthy is that the time dependence of the LSPR wavelength for HfO_2-clad Ag, when placed in a

https://doi.org/10.1021/acs.jpcc.1c04599
J. Phys. Chem. C 2021, 125, 17212−17220

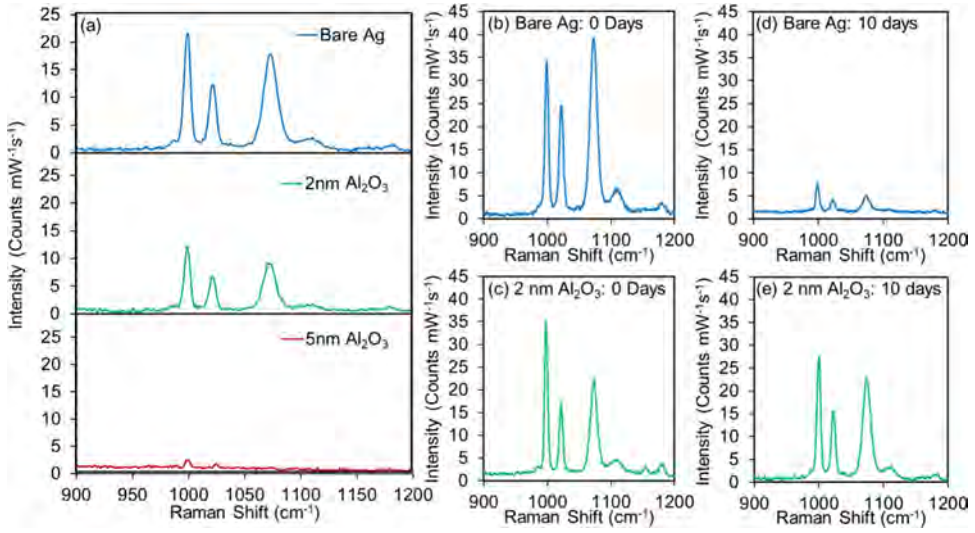

Figure 5. (a) SERS spectra for thiophenol detection for bare Ag nanostructures and identical structures clad with 2 and 5 nm of ALD-deposited Al_2O_3. SERS spectra showing the thiophenol peaks derived from freshly prepared (b) bare Ag nanostructures and (c) identical structures with a 2 nm thick Al_2O_3 cladding and the same (d) bare and (e) clad structures measured 10 days later.

highly acidic environment, shows values that are considerably more stable than those obtained for samples placed in H_2O or NaOH. This is likely attributable to acidic conditions maintaining a clean HfO_2 surface. As anticipated, Al_2O_3- and TiO_2-clad Ag structures, which performed relatively poorly in H_2O, showed an even more rapid rate of deterioration when exposed to these extreme pH environments (Figure S3b,c). ALD-deposited Al_2O_3 proved extremely vulnerable under basic conditions,[43,54,69] seeing the 5 nm layer completely etched after 8 min for a NaOH concentration of only 1 mM.

SERS Activity of Bare and Al_2O_3-Clad Ag Nanostructures. Numerous techniques are emerging in which nanometal syntheses are integrated with ALD oxide depositions to form hybrid plasmonic materials of relevance to SERS applications.[72] When plasmonic structures are coated with ultrathin ALD-deposited layers, they diminish the electromagnetic near fields accessible for SERS enhancements. Nonetheless, the oxide provides a protective coating that can enhance the chemical stability and durability of the SERS surface, properties of consequence because they allow for SERS measurements in chemically aggressive environments, an increased shelf life, and recyclability of the SERS substrate. As such, a branch of SERS sensing, referred to as shell-isolated nanoparticle-enhanced Raman spectroscopy (SHINERS), has emerged that aims to exploit these advantages.[1−4] Studies were, therefore, carried out to determine whether Al_2O_3-clad Ag structures are amenable to the SHINERS modality where the goal is to demonstrate functionality rather than create a SERS substrate with a large enhancement.

Measurements were carried out that compare the (i) SERS spectra derived from bare Ag to that obtained for identical nanostructures clad with Al_2O_3 layer thicknesses of 2 and 5 nm and (ii) SERS aging characteristics for bare Ag and identical structures with a 2 nm cladding. Thiophenol was used as the SERS probe molecule, where three well-established peaks located at 999, 1022, and 1074 cm^{-1} were monitored.[73] For both comparisons, all common synthesis and processing steps, as well as the application of thiophenol, were, to the extent possible, carried out together to minimize sample-to-sample variations. Figure 5a shows the influence of the Al_2O_3 cladding on the SERS spectrum. As anticipated, it reveals three prominent thiophenol peaks that diminish in amplitude as the cladding thickness is increased. The data highlights the need for thin protective coatings since the 2 nm thick cladding displays distinct peaks, whereas they are barely discernible when the cladding thickness is increased to 5 nm. The result is consistent with simulations showing the influence of shell thickness on the plasmonic near fields.[7,38] The aging characteristics of both the bare and clad structures were characterized by measuring the SERS spectra of freshly prepared samples along with identical samples aged in air for 10 days prior to the measurement. The spectra, which are shown in Figure 5b−e, clearly show that unprotected Ag exhibits a greatly diminished SERS signal, whereas the Al_2O_3-clad structure maintains its SERS enhancement to values consistent with sample-to-sample variations. It should be noted that after 10 days of aging, the SERS signal for the Al_2O_3-clad structures greatly exceeds that of the unprotected Ag. Collectively, this data demonstrates the overall appeal of the SHINERS approach in that there exists a trade-off that sees the SERS signal sacrificed for an improvement in the stability of the SERS substrate.

■ DISCUSSION

Ag nanostructure synthesis and ALD, when practiced in combination, have the potential to create integrated solutions that are tuned for the stability−property relationships that best fit the needs of a specific application. The approach takes advantage of the fine controls offered by the ALD layer-by-layer conformal growth mode while simultaneously using the internal Ag structure as a built-in plasmonic sensor for assessing shell durability. The rational design of such structures is further enhanced by the amenability of the ALD technique to the deposition of a broad range of highly stable oxide and nitride cladding materials, where each has its own distinct character. With such versatility, there exists an expansive design space where exacting controls over shell thickness and material uniformity should allow for simulations that accurately reflect experimental configurations. Even though the current work utilized dewetted Ag nanostructures with a single-crystal

https://doi.org/10.1021/acs.jpcc.1c04599
J. Phys. Chem. C 2021, 125, 17212−17220

character, these same techniques should also be applicable to Ag nanostructures formed by lithographic procedures. ALD does, however, have its drawbacks. The fact that depositions typically require the use of somewhat elevated temperatures could prove problematic when trying to preserve Ag nanostructure geometries with sharp corners (e.g., nanoprisms). It is also a point of concern that Ag shows sensitivity to humidity, yet H_2O is often used as a reductant in the ALD process. It, therefore, cannot be ruled out that Ag nanostructures undergo some level of degradation in the early stages of the ALD deposition. Additionally, ALD, while ideally suited for the protection of substrate-based structures, is not well-suited for stabilizing structures derived from colloidal syntheses. Any nanostructure syntheses utilizing capping agents would also require their removal prior to application of the ALD cladding.

Within the context of the current results, there are also a number of specific takeaways in terms of advancing shell-isolated plasmonic nanostructures reliant on ALD-deposited claddings. Important is that pinhole-free oxide claddings are able to sustain plasmonic properties in air for durations of significance to applications requiring long-term usage and extended shelf lives. Additionally, ALD-deposited layers as thin as 1 nm, which are known to have pinholes, provide protection in air for at least 40 days without a significant deterioration in plasmonic properties, a result of high significance from the standpoint of having electromagnetic near fields that extend beyond the spatial extent of the cladding.[7,38] The result forwards the possibility of using oxide-clad structures in SERS sensing schemes where the analyte is adsorbed onto the oxide surface. Aqueous solutions provide a more challenging environment for shell-isolated Ag nanostructures but where HfO_2 stands out as impervious, even when exposed to extreme pH environments. The vulnerability of Al_2O_3 claddings in low concentrations of NaOH (i.e., 1 mM), while seemingly disadvantageous, could potentially be exploited in that it provides the means for protecting Ag nanostructures from air up until their point of use, at which time, the coating can be selectively removed. In doing so, it would provide a long duration shelf life while allowing for the onetime use of freshly exposed Ag nanostructures. On a cautionary note, the results also reveal that airborne impurities can adsorb onto ALD-deposited oxide layers. This can cause slight shifts in the LSPR even though the Ag nanostructure remains protected. For the case of TiO_2 claddings, however, the situation is easily remedied by illuminating the structures with UV light prior to usage.

CONCLUSIONS

In summary, this study has demonstrated ALD-deposited oxide claddings as an effective means for forming shell-isolated Ag nanostructures that retain important plasmonic properties while mitigating environmental sensitivities. It also demonstrates ALD as a versatile platform for designing claddings that are responsive to the needs of specific applications. With Ag being an impressive yet underutilized plasmonic material, the work contributes to an effort that could see Ag regain its luster as a plasmonic material suitable for real-world applications.

ASSOCIATED CONTENT

Supporting Information

The Supporting Information is available free of charge at https://pubs.acs.org/doi/10.1021/acs.jpcc.1c04599.

Additional Ag nanostructure characterization and endurance testing data for oxide-clad structures (PDF)

AUTHOR INFORMATION

Corresponding Author

Svetlana Neretina − *College of Engineering and Department of Chemistry & Biochemistry, University of Notre Dame, Notre Dame, Indiana 46556, United States;* orcid.org/0000-0002-6889-4384; Email: sneretina@nd.edu

Authors

Arin S. Preston − *College of Engineering, University of Notre Dame, Notre Dame, Indiana 46556, United States*

Robert A. Hughes − *College of Engineering, University of Notre Dame, Notre Dame, Indiana 46556, United States*

Nathaniel L. Dominique − *Department of Chemistry & Biochemistry, University of Notre Dame, Notre Dame, Indiana 46556, United States;* orcid.org/0000-0002-0439-9982

Jon P. Camden − *Department of Chemistry & Biochemistry, University of Notre Dame, Notre Dame, Indiana 46556, United States;* orcid.org/0000-0002-6179-2692

Complete contact information is available at: https://pubs.acs.org/10.1021/acs.jpcc.1c04599

Notes

The authors declare no competing financial interest.

ACKNOWLEDGMENTS

This work is supported by the National Science Foundation Awards to S.N. (CMMI-1911991) and J.P.C. (CHE-204171). It has also benefited from the facilities available through the Notre Dame Nanofabrication Facility (NDNF) and the Notre Dame Integrated Imaging Facility (NDIIF). The authors acknowledge the expertise of M. Richmond in the preparation of ALD claddings.

REFERENCES

(1) Li, J.-F.; Zhang, Y.-J.; Ding, S.-Y.; Panneerselvam, R.; Tian, Z. Q. Core−Shell Nanoparticle-Enhanced Raman Spectroscopy. *Chem. Rev.* **2017**, *117*, 5002−5069.

(2) Krajczewski, J.; Kudelski, A. Shell-Isolated Nanoparticle-Enhanced Raman Spectroscopy. *Front. Chem.* **2019**, *7*, No. 410.

(3) Li, C.; Jin, Y. Shell-Isolated Plasmonic Nanostructures for Biosensing, Catalysis, and Advanced Nanoelectronics. *Adv. Funct. Mater.* **2021**, *31*, No. 2008031.

(4) Langer, J.; de Aberasturi, D. J.; Aizpurua, J.; Alvarez-Puebla, R. A.; Auguié, B.; Baumberg, J. J.; Bazan, G. C.; Bell, S. E. J.; Boisen, A.; Brolo, A. G.; et al. Present and Future of Surface-Enhanced Raman Scattering. *ACS Nano* **2020**, *14*, 28−117.

(5) Li, J.-F.; Li, C.-Y.; Aroca, R. F. Plasmon-Enhanced Fluorescence Spectroscopy. *Chem. Soc. Rev.* **2017**, *46*, 3962−3979.

(6) Dong, J.; Zhang, Z.; Zheng, H.; Sun, M. Recent Progress on Plasmon-Enhanced Fluorescence. *Nanophotonics* **2015**, *4*, 472−490.

(7) Preston, A. S.; Hughes, R. A.; Demille, T. B.; Neretina, S. Plasmonics Under Attack: Protecting Copper Nanostructures from Harsh Environments. *Chem. Mater.* **2020**, *32*, 6788−6799.

(8) Albrecht, G.; Ubl, M.; Kaiser, S.; Giessen, H.; Hentschel, M. Comprehensive Study of Plasmonic Materials in the Visible and Near-Infrared: Linear, Refractory, and Nonlinear Optical Properties. *ACS Photonics* **2018**, *5*, 1058−1067.

(9) Albrecht, G.; Kaiser, S.; Giessen, H.; Hentschel, M. Refractory Plasmonics without Refractory Materials. *Nano Lett.* **2017**, *17*, 6402−6408.

(10) West, P. R.; Ishii, S.; Naik, G. V.; Emani, N. K.; Shalaev, V. M.; Boltasseva, A. Searching for Better Plasmonic Materials. *Laser Photonics Rev.* **2010**, *4*, 795−808.
(11) Mayer, K. M.; Hafner, J. H. Localized Surface Plasmon Resonance Sensors. *Chem. Rev.* **2011**, *111*, 3828−3857.
(12) Rycenga, M.; Cobley, C. M.; Zeng, J.; Li, W.; Moran, C. H.; Zhang, Q.; Qin, D.; Xia, Y. Controlling the Synthesis and Assembly of Silver Nanostructures for Plasmonic Applications. *Chem. Rev.* **2011**, *111*, 3669−3712.
(13) Hajfathalian, M.; Gilroy, K. D.; Hughes, R. A.; Neretina, S. Citrate-Induced Nanocubes: A Reexamination of the Role of Citrate as a Shape-Directing Capping Agent for Ag-Based Nanostructures. *Small* **2016**, *12*, 3444−3452.
(14) Preston, A. S.; Hughes, R. A.; Demille, T. B.; Rey Davila, V. M.; Neretina, S. Dewetted Nanostructures of Gold, Silver, Copper, and Palladium with Enhanced Faceting. *Acta Mater.* **2019**, *165*, 15−25.
(15) Ma, L.; Huang, Y.; Hou, M.; Xie, Z.; Zhang, Z. Silver Nanorods Wrapped with Ultrathin Al_2O_3 Layers Exhibiting Excellent SERS Sensitivity and Outstanding SERS Stability. *Sci. Rep.* **2015**, *5*, No. 12890.
(16) Demille, T. B.; Hughes, R. A.; Neretina, S. Periodic Arrays of Dewetted Silver Nanostructures on Sapphire and Quartz: Effect of Substrate Truncation on the Localized Surface Plasmon Resonance and Near-Field Enhancement. *J. Phys. Chem. C* **2019**, *123*, 19879−19886.
(17) Farzinpour, P.; Sundar, A.; Gilroy, K. D.; Eskin, Z. E.; Hughes, R. A.; Neretina, S. Altering the Dewetting Characteristics of Ultrathin Gold and Silver Films using a Sacrificial Antimony Layer. *Nanotechnology* **2012**, *23*, No. 495604.
(18) Scuderi, M.; Esposito, M.; Todisco, F.; Simeone, D.; Tarantini, I.; De Marco, L.; De Giorgi, M.; Nicotra, G.; Carbone, L.; Sanvitto, D.; et al. Nanoscale Study of the Tarnishing Process in Electron Beam Lithography-Fabricated Silver Nanoparticles for Plasmonic Applications. *J. Phys. Chem. C* **2016**, *120*, 24314−24323.
(19) Losurdo, M.; Bergmair, I.; Giangregorio, M. M.; Dastmalchi, B.; Bianco, G. V.; Helgert, C.; Pshenay-Severin, E.; Falkner, M.; Pertsch, T.; Kley, E.-B.; et al. Enhancing Chemical and Optical Stability of Silver Nanostructures by Low-Temperature Hydrogen Atoms Processing. *J. Phys. Chem. C* **2012**, *116*, 23004−23012.
(20) Oates, T. W. H.; Losurdo, M.; Noda, S.; Hinrichs, K. The Effect of Atmospheric Tarnishing on the Optical and Structural Properties of Silver Nanoparticles. *J. Phys. D: Appl. Phys.* **2013**, *46*, No. 145308.
(21) Grillet, N.; Manchon, D.; Cottancin, E.; Bertorelle, F.; Bonnet, C.; Broyer, M.; Lermé, J.; Pellarin, M. Photo-Oxidation of Individual Silver Nanoparticles: A Real-Time Tracking of Optical and Morphological Changes. *J. Phys. Chem. C* **2013**, *117*, 2274−2282.
(22) Han, Y.; Lupitskyy, R.; Chou, T.-M.; Stafford, C. M.; Du, H.; Sukhishvili, S. Effect of Oxidation on Surface-Enhanced Raman Scattering Activity of Silver Nanoparticles: A Quantitative Correlation. *Anal. Chem.* **2011**, *83*, 5873−5880.
(23) Cao, W.; Elsayed-Ali, H. E. Stability of Ag Nanoparticles Fabricated by Electron Beam Lithography. *Mater. Lett.* **2009**, *63*, 2263−2266.
(24) McMahon, M. D.; Lopez, R.; Meyer, H. M.; Feldman, L. C.; Haglund, R. F. Rapid Tarnishing of Silver Nanoparticles in Ambient Laboratory Air. *Appl. Phys. B: Lasers Opt.* **2005**, *80*, 915−921.
(25) Wang, X.; Santschi, C.; Martin, O. J. F. Strong Improvement of Long-Term Chemical and Thermal Stability of Plasmonic Silver Nanoantennas and Films. *Small* **2017**, *13*, No. 700044.
(26) Graedel, T. E.; Franey, J. P.; Gualtieri, G. J.; Kammlott, G. W.; Malm, D. L. On the Mechanism of Silver and Copper Sulfidation by Atmospheric H_2S and OCS. *Corros. Sci.* **1985**, *25*, 1163−1180.
(27) Matikainen, A.; Nuutinen, T.; Itkonen, T.; Heinilehto, S.; Puustinen, J.; Hiltunen, J.; Lappalainen, J.; Karioja, P.; Vahimaa, P. Atmospheric Oxidation and Carbon Contamination of Silver and its Effect on Surface-Enhanced Raman Spectroscopy (SERS). *Sci. Rep.* **2016**, *6*, No. 37192.
(28) Menumerov, E.; Hughes, R. A.; Golze, S. D.; Neal, R. D.; Demille, T. B.; Campanaro, J. C.; Kotesky, K. C.; Rouvimov, S.; Neretina, S. Identifying the True Catalyst in the Reduction of 4-Nitrophenol: A Case Study Showing the Effect of Leaching and Oxidative Etching Using Ag Catalysts. *ACS Catal.* **2018**, *8*, 8879−8888.
(29) Mikhlin, Y. L.; Vishnyakova, E. A.; Romanchenko, A. S.; Saikova, S. V.; Likatski, M. N.; Larichev, Y. V.; Tuzikov, F. V.; Zaikovskii, V. I.; Zharkov, S. M. Oxidation of Ag Nanoparticles in Aqueous Media: Effect of Particle Size and Capping. *Appl. Surf. Sci.* **2014**, *297*, 75−83.
(30) Chen, Y.; Wang, C.; Ma, Z.; Su, Z. Controllable Colours and Shapes of Silver Nanostructures Based on pH: Application to Surface-Enhanced Raman Scattering. *Nanotechnology* **2007**, *18*, No. 325602.
(31) Johnston, K. A.; Stabryla, L. M.; Smith, A. M.; Gan, X. Y.; Gilbertson, L. M.; Millstone, J. E. Impacts of Broth Chemistry on Silver Ion Release, Surface Chemistry Composition, and Bacterial Cytotoxicity of Silver Nanoparticles. *Environ. Sci.: Nano* **2018**, *5*, 304−312.
(32) Lee, K. E.; Hesketh, A. V.; Kelly, T. L. Chemical Stability and Degradation Mechanisms of Triangular Ag, Ag@Au and Au Nanoprisms. *Phys. Chem. Chem. Phys.* **2014**, *16*, 12407.
(33) Tang, B.; Xu, S.; Hou, X.; Li, J.; Sun, L.; Xu, W.; Wang, X. Shape Evolution of Silver Nanoplates through Heating and Photoinduction. *ACS Appl. Mater. Interfaces* **2013**, *5*, 646−653.
(34) Kang, H.; Buchman, J. T.; Rodriguez, R. S.; Ring, H. L.; He, J.; Bantz, K. C.; Haynes, C. L. Stabilization of Silver and Gold Nanoparticles: Preservation and Improvement of Plasmonic Functionalities. *Chem. Rev.* **2019**, *119*, 664−699.
(35) Zhou, Y.; Liang, P.; Zhang, D.; Tang, L.; Dong, Q.; Jin, S.; Ni, D.; Yu, Z.; Ye, J. A Facile Seed Growth Method to Prepare Stable Ag@ZrO_2 Core−Shell SERS Substrate With High Stability in Extreme Environments. *Spectrochim. Acta, Part A* **2020**, *228*, No. 117676.
(36) Yang, P.-S.; Yin, Y.-T.; Lin, P.-C.; Chen, L.-Y.; Chen, M.-J. High Chemical Resistance and Raman Enhancement in Ag/Al_2O_3 Core−Shell Plasmonic Nanostructures Tailored by Atomic Layer Deposition. *Mater. Chem. Phys.* **2019**, *223*, 441−446.
(37) Yang, Y.; Liu, J.; Fu, Z. W.; Qin, D. Galvanic Replacement-Free Deposition of Au on Ag for Core−Shell Nanocubes with Enhanced Chemical Stability and SERS Activity. *J. Am. Chem. Soc.* **2014**, *136*, 8153−8156.
(38) Asapu, R.; Claes, N.; Bals, S.; Denys, S.; Detavernier, C.; Lenaerts, S.; Verbruggen, S. Silver-Polymer Core−Shell Nanoparticles for Ultrastable Plasmon-Enhanced Photocatalysis. *Appl. Catal., B* **2017**, *200*, 31−38.
(39) Scarabelli, L.; Schumacher, M.; Jimenez de Aberasturi, D.; Merkl, J.-P.; Henriksen-Lacey, M.; Milagres de Oliveira, T.; Janschel, M.; Schmidtke, C.; Bals, S.; Weller, H.; et al. Encapsulation of Noble Metal Nanoparticles through Seeded Emulsion Polymerization as Highly Stable Plasmonic Systems. *Adv. Funct. Mater.* **2019**, *29*, No. 1809071.
(40) Jiang, X.; Zeng, Q.; Yu, A. Thiol-Frozen Shape Evolution of Triangular Silver Nanoplates. *Langmuir* **2007**, *23*, 2218−2223.
(41) Lee, B.-H.; Hsu, M.-S.; Hsu, Y.-C.; Lo, C.-W.; Huang, C.-L. A Facile Method to Obtain Highly Stable Silver Nanoplate Colloids with Desired Surface Plasmon Resonance Wavelengths. *J. Phys. Chem. C* **2010**, *114*, 6222−6227.
(42) El Wanees, S. A.; El Aal Mohamed, A. A.; El Azeem, M. A.; El Said, R. Inhibition of Silver Corrosion in Nitric Acid by Some Aliphatic Amines. *J. Dispersion Sci. Technol.* **2010**, *31*, 1516−1525.
(43) Guay, J.; Killaire, G.; Gordon, P.; Barry, S.; Berini, P.; Weck, A. Passivation of Plasmonic Colors on Bulk Silver by Atomic Layer Deposition of Aluminum Oxide. *Langmuir* **2018**, *34*, 4998−5010.
(44) Ma, L.; Huang, Y.; Hou, M.; Xie, Z.; Zhang, Z. Ag Nanorods Coated with Ultrathin TiO_2 Shells as Stable and Recyclable SERS Substrates. *Sci. Rep.* **2015**, *5*, No. 15442.
(45) Higashino, M.; Murai, S.; Tanaka, K. Improving the Plasmonic Response of Silver Nanoparticle Arrays via Atomic Layer Deposition

Coating and Annealing above the Melting Point. *J. Phys. Chem. C* **2020**, *124*, 27687−27693.
(46) Sung, J.; Kosuda, K. M.; Zhao, J.; Elam, J. W.; Spears, K. G.; Van Duyne, R. P. Stability of Silver Nanoparticles Fabricated by Nanosphere Lithography and Atomic Layer Deposition to Femtosecond Laser Excitation. *J. Phys. Chem. C* **2008**, *112*, 5707−5714.
(47) Nugroho, F. A. A.; Albinsson, D.; Antosiewicz, T. J.; Langhammer, C. Plasmonic Metasurface for Spatially Resolved Optical Sensing in Three Dimensions. *ACS Nano* **2020**, *14*, 2345−2353.
(48) Losurdo, M.; Bergmair, I.; Dastmalchi, B.; Kim, T.-H.; Giangregroio, M. M.; Jiao, W.; Bianco, G. V.; Brown, A. S.; Hingerl, K.; Bruno, G. Graphene as an Electron Shuttle for Silver Deoxidation: Removing a Key Barrier to Plasmonics and Metamaterials for SERS in the Visible. *Adv. Funct. Mater.* **2014**, *24*, 1864−1878.
(49) Reed, J. C.; Zhu, H.; Zhu, A. Y.; Li, C.; Cubukcu, E. Graphene-Enabled Silver Nanoantenna Sensors. *Nano Lett.* **2012**, *12*, 4090−4094.
(50) Bosman, M.; Zhang, L.; Duan, H.; Tan, S. F.; Nijhuis, C. A.; Qiu, C.; Yang, J. K. W. Encapsulated Annealing: Enhancing the Plasmon Quality Factor in Lithographically-Defined Nanostructures. *Sci. Rep.* **2015**, *4*, No. 5537.
(51) Johnson, R. W.; Hultqvist, A.; Bent, S. F. A Brief Review of Atomic Layer Deposition: From Fundamentals to Applications. *Mater. Today* **2014**, *17*, 236−246.
(52) McNeary, W. W.; Linico, A. E.; Ngo, C.; Van Rooji, S.; Haussener, S.; Maguire, M. E.; Pylypenko, S.; Weimer, A. W. Atomic Layer Deposition of TiO_2 for Stabilization of Pt Nanoparticle Oxygen Reduction Reaction Catalysts. *J. Appl. Electrochem.* **2018**, *48*, 973−984.
(53) Daubert, J. S.; Hill, G. T.; Gotsch, H. N.; Gremaud, A. P.; Ovental, J. S.; Williams, P. S.; Oldham, C. J.; Parsons, G. N. Corrosion Protection of Copper Using Al_2O_3, TiO_2, ZnO, HfO_2, and ZrO_2 Atomic Layer Deposition. *ACS Appl. Mater. Interfaces* **2017**, *9*, 4192−4201.
(54) Marquardt, A. E.; Breitung, E. M.; Drayman-Weisser, T.; Gates, G.; Phanuef, R. J. Protecting Silver Cultural Heritage Objects with Atomic Layer Deposited Corrosion Barriers. *Heritage Sci.* **2015**, *3*, No. 37.
(55) Grimm, O. C.; Dulanga, R. M.; Somaratne, S.; Wang, Y.; Kim, S.; Whitten, J. E. Thiol Adsorption on Metal Oxide Nanoparticles. *Phys. Chem. Chem. Phys.* **2021**, *23*, 8309−8317.
(56) Gu, X.; Trujillo, M. J.; Olson, J. E.; Camden, J. P. SERS Sensors: Recent Developments and a Generalized Classification Scheme Based on the Signal Origin. *Annu. Rev. Anal. Chem.* **2018**, *11*, 147−169.
(57) Watson, G. H.; Daniels, W. B.; Wang, C. S. Measurements of Raman Intensities and Pressure Dependence of Phonon Frequencies in Sapphire. *J. Appl. Phys.* **1981**, *52*, 956−958.
(58) Gilroy, K. D.; Farzinpour, P.; Sundar, A.; Tan, T.; Hughes, R. A.; Neretina, S. Substrate-Based Galvanic Replacement Reactions Carried out on Heteroepitaxially Formed Silver Templates. *Nano Res.* **2013**, *6*, 418−428.
(59) Gilroy, K. D.; Sundar, A.; Farzinpour, P.; Hughes, R. A.; Neretina, S. Mechanistic Study of Substrate-Based Galvanic Replacement Reactions. *Nano Res.* **2014**, *7*, 365−379.
(60) Chen, H.; Kou, X.; Yang, Z.; Ni, W.; Wang, J. Shape- and Size-Dependent Refractive Index Sensitivity of Gold Nanoparticles. *Langmuir* **2008**, *24*, 5233−5237.
(61) Mahmoud, M. A.; Chamanzar, M.; Adibi, A.; El-Sayed, M. A. Effect of the Dielectric Constant of the Surrounding Medium and the Substrate on the Surface Plasmon Resonance Spectrum and Sensitivity Factors of Highly Symmetric Systems: Silver Nanocubes. *J. Am. Chem. Soc.* **2012**, *134*, 6434−6442.
(62) Mazzotta, F.; Johnson, T.; Dahlin, A.; Shaver, J.; Oh, S.; Höök, F. Influence of the Evanescent Field Decay Length on the Sensitivity of Plasmonic Nanodisks and Nanoholes. *ACS Photonics* **2015**, *2*, 256−262.
(63) Mock, J.; Smith, D.; Shultz, S. Local Refractive Index Dependence of Plasmon Resonance Spectra from Individual Nanoparticles. *Nano Lett.* **2003**, *3*, 485−491.
(64) Long, R.; Zhou, S.; Wiley, B. J.; Xiong, Y. Oxidative Etching for Controlled Synthesis of Metal Nanocrystals: Atomic Addition and Subtraction. *Chem. Soc. Rev.* **2014**, *43*, 6288−6310.
(65) Zheng, Y.; Zeng, J.; Ruditskiy, A.; Liu, M.; Xia, Y. Oxidative Etching and Its Role in Manipulating the Nucleation and Growth of Noble-Metal Nanocrystals. *Chem. Mater.* **2014**, *26*, 22−33.
(66) Toh, H. S.; Jurkschat, K.; Compton, R. G. The Influence of the Capping Agent on the Oxidation of Silver Nanoparticles: Nano-impacts versus Stripping Voltammetry. *Chem. - Eur. J.* **2015**, *21*, 2998−3004.
(67) Wang, P.; Bai, Y.; Luo, P.; Liu, J. Ag_2O/Ag_3PO_4 Heterostructures: Highly Efficient and Stable Visible-Light-Induced Photocatalyst for Degradation of Methyl Orange and Phenol. *Micro Nano Lett.* **2013**, *8*, 340−344.
(68) Gao, Y.; Feng, H.; Ma, J.; Zhang, Z.; Lu, J.; Chen, Y.; Yang, S.; Gu, J. Analysis of the Dielectric Constants of the Ag_2O Film by Spectroscopic Ellipsometry and Single-Oscillator Model. *Phys. B* **2010**, *405*, 1922−1926.
(69) Correa, G. C.; Bao, B.; Strandwitz, N. C. Chemical Stability of Titania and Alumina Thin Films Formed by Atomic Layer Deposition. *ACS Appl. Mater. Interfaces* **2015**, *7*, 14816−14821.
(70) Li, M.; Jin, Z.; Bai, Y.; Cao, Y.; Li, W.; Wu, D.; Li, A. Comparison of Chemical Stability and Corrosion Resistance of Group IV Metal Oxide Films formed by Thermal and Plasma-Enhanced Atomic Layer Deposition. *Sci. Rep.* **2019**, *9*, No. 10438.
(71) Singh, A. K.; Adstedt, K.; Brown, B.; Singh, P. M.; Graham, S. Development of ALD Coatings for Harsh Environment Applications. *ACS Appl. Mater. Interfaces* **2019**, *11*, 7498−7509.
(72) Prakash, J.; Swart, H. C.; Zhang, G.; Sun, S. Emerging Applications of Atomic Layer Deposition for the Rational Design of Novel Nanostructures for Surface-Enhanced Raman Scattering. *J. Mater. Chem. C* **2019**, *7*, 1447−1471.
(73) Li, S.; Wu, D.; Xu, X.; Gu, R. Theoretical and Experimental Studies on the Adsorption Behavior of Thiophenol on Gold Nanoparticles. *J. Raman Spectrosc.* **2007**, *38*, 1436−1443.

https://doi.org/10.1021/acs.jpcc.1c04599
J. Phys. Chem. C 2021, 125, 17212−17220